Journal of Physics: Conference Series **489** (2014) 012076 doi:10.1088/1742-6596/489/1/012076

Segmentation of cone-beam CT using a hidden Markov random field with informative priors

M Moores[1,3], C Hargrave[1,2,3], F Harden[1,3] and K Mengersen[1,3]

[1] Queensland University of Technology, Brisbane QLD 4000 Australia
[2] Radiation Oncology Mater Centre, Queensland Health, South Brisbane QLD 4101 Australia
[3] Institute of Health and Biomedical Innovation, Kelvin Grove QLD 4059 Australia

E-mail: matthew.moores@qut.edu.au

Abstract. Cone-beam computed tomography (CBCT) has enormous potential to improve the accuracy of treatment delivery in image-guided radiotherapy (IGRT). To assist radiotherapists in interpreting these images, we use a Bayesian statistical model to label each voxel according to its tissue type. The rich sources of prior information in IGRT are incorporated into a hidden Markov random field model of the 3D image lattice. Tissue densities in the reference CT scan are estimated using inverse regression and then rescaled to approximate the corresponding CBCT intensity values. The treatment planning contours are combined with published studies of physiological variability to produce a spatial prior distribution for changes in the size, shape and position of the tumour volume and organs at risk. The voxel labels are estimated using iterated conditional modes. The accuracy of the method has been evaluated using 27 CBCT scans of an electron density phantom. The mean voxel-wise misclassification rate was 6.2%, with Dice similarity coefficient of 0.73 for liver, muscle, breast and adipose tissue. By incorporating prior information, we are able to successfully segment CBCT images. This could be a viable approach for automated, online image analysis in radiotherapy.

1. Introduction

Due to the level of precision and detail required for sufficient volume variation analysis of daily cone-beam CT (CBCT), coupled with the short timeframe in which the radiotherapy procedure is to be carried out in the clinic, radiation therapists are currently unable to perform a detailed analysis of the CBCT scans prior to irradiation. Automated methods may aid in the decision-making process by labelling the image voxels according to tissue type, estimating the boundaries of the tumour and neighbouring organs, and highlighting any regions where changes in these boundaries might have exceeded tolerance. Multi-thresholding using an independent Gaussian mixture model (GMM) is error-prone due to the low contrast-to-noise ratio (CNR) in CBCT scans of human tissue. The low CNR is exemplified by the axial slice from a CBCT shown in figure 1. For comparison, a fan-beam (FBCT) scan of the same subject is illustrated in figure 2. The voxel intensity values alone are insufficient to accurately segment the image according to tissue type; therefore more complex methods are necessary.

Recent approaches to boundary estimation in CBCT have used deformable models that evolve according to partial differential equations. The two major approaches are 3D mesh models [1] and level sets [2]. These models need to be initialized very close to the boundary of interest, as they are prone to becoming stuck on local minima. Thus, they are more suited as a post-processing

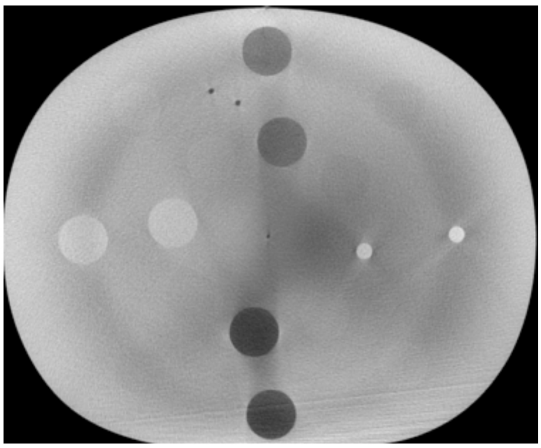

Figure 1. CBCT scan of the ED phantom.

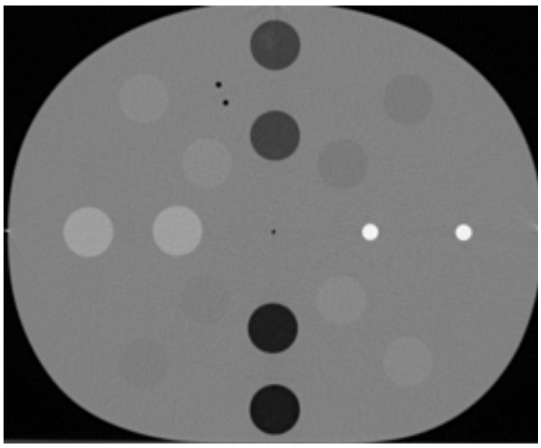

Figure 2. FBCT scan of the ED phantom.

step to refine an approximate solution that was obtained via other means, as in [3, 4, 5]. Other approaches include hidden Markov random field (MRF) models and graph-based segmentation. It has been shown that segmentation by graph cut is equivalent to fitting a discrete MRF [6], so these are essentially two different approaches with the same underlying model.

In this paper we introduce new methods for utilising the rich sources of prior information that are available in IGRT by extending the hidden MRF model. We demonstrate these methods on CBCT scans of an electron density (ED) phantom and show that the external field prior results in a substantial improvement in segmentation accuracy.

2. Materials and Methods

The planning CT along with the contours of the gross tumour volume (GTV) and organs at risk (OAR) constitute a valuable source of prior information for analysing CBCT scans. They can be viewed as a snapshot of the patient at a previous point in time. This patient-specific information can be combined with published studies of organ motion and setup error to produce a probabilistic spatial distribution of voxel labels. The spatial distribution is computed relative to the scan isocentre, avoiding the need for a separate registration step.

2.1. ED phantom experiment

We have evaluated the performance of our method using CBCT scans of a tissue-equivalent ED phantom (CIRS, Inc. model 062). The ED phantom was manufactured from epoxy and contains cylindrical inserts that mimic the X-ray absorption of human tissue: lung (inhale); lung (exhale); adipose; breast (50% fat); water-equivalent solid; muscle; liver; spongy (trabecular) bone; and dense (cortical) bone. The CBCT scans were acquired from a Varian linear accelerator with On-Board Imager (OBI) using a half bow-tie filter to achieve a 450mm field of view. 53 CBCT scans were obtained in total, with 27 held out for testing and 26 incorporated into the Bayesian prior. We also acquired 28 FBCT scans of the same phantom from a Siemens SOMATOM Sensation Open. These scans represent prior information, as will be explained in section 2.2. Example CBCT and FBCT scans of the ED phantom are illustrated in figures 1 and 2.

2.2. Informative priors for CT number

CBCT scanners are not calibrated to the Hounsfield scale. Nevertheless, there is a linear relationship between electron density in a homogeneous region of tissue and the mean intensity

of the corresponding voxel values [7]. This relationship has been quantified by fitting a regression model to 26 CBCT scans of the ED phantom. We were thus able to rescale estimates of tissue density from a patient's planning CT scan to predict the distribution of intensity values in a CBCT scan of the same patient. These estimates were incorporated into the hidden MRF model as priors for the mean and variance of each mixture component [8].

2.3. External field prior for voxel labels

We have also included spatial prior information in the MRF model, in the form of an external field. The external field was centred on the planning contours of the GTV and the OARs, relative to the scan isocentre. Geometric uncertainty was incorporated into the model using quantifications of organ motion from published studies. For our ED phantom experiment, we used a mean displacement of 1.2mm with a standard deviation of 7.3mm, which is typical of prostate motion [9]. The external field prior for the ED phantom is illustrated in figure 3.

2.4. Iterated conditional modes

We used the iterated conditional modes (ICM) algorithm [10] to fit our hidden MRF model. This algorithm was implemented by modifying the source code of the R package mritc [11] to accommodate the external field prior and to support a 9 component mixture model.

3. Results and discussion

We first estimated the relationship between electron density ($\times 10^{23}$/cc) and voxel intensity. By fitting the regression model to 26 CBCT scans, we obtained posterior means of 152 for the slope and -761 for the intercept, with standard deviations of 0.97 and 0.30 respectively. Tissue densities were estimated from the 28 FBCT scans and then rescaled using the regression equation to obtain prior distributions for the voxel intensities. This regression relationship is specific to the CBCT scanner in question, but it would be straightforward to fit the same regression model to each on-board imaging device in the radiotherapy department.

The remaining 27 CBCT scans were segmented using between 34 and 100 iterations of the ICM algorithm. This took an average of 9 minutes per scan, running in a single thread. We anticipate that a parallel implementation of the ICM algorithm could reduce this execution time substantially. Overall, the mean misclassification rate was 6.4%. An example image segmentation is shown in figure 4. Table 1 shows a breakdown of segmentation accuracy by tissue type, measured using Dice similarity coefficients [12].

Table 1. Average segmentation accuracy for 27 CBCT scans.

Tissue Type	Dice ($\pm\sigma$)
Lung (inhale)	0.886 ± 0.010
Lung (exhale)	0.805 ± 0.024
Adipose	0.741 ± 0.039
Breast	0.721 ± 0.036
Water	0.964 ± 0.004
Muscle	0.728 ± 0.052
Liver	0.737 ± 0.035
Spongy bone	0.755 ± 0.022
Dense bone	0.723 ± 0.066

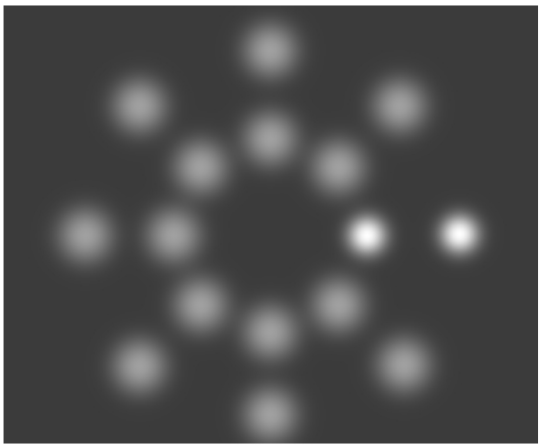

Figure 3. External field prior.

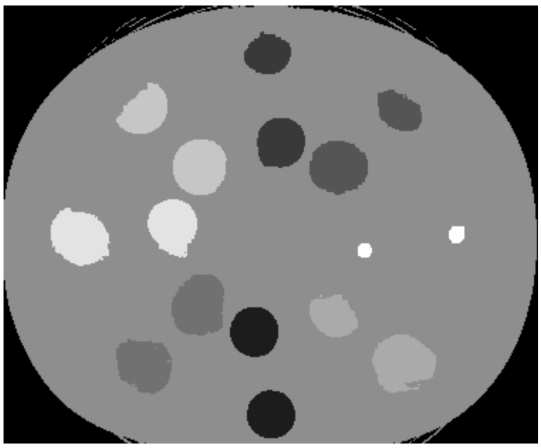

Figure 4. Segmentation result.

4. Conclusion

The external field prior substantially improves segmentation accuracy by incorporating additional spatial information into the model. We have demonstrated this method by application to CBCT scans of an ED phantom so that we are able to evaluate segmentation accuracy against the ground truth. The next step will be to apply the method to radiotherapy patient data.

Acknowledgments

This research is part of a collaborative project between Queensland University of Technology (QUT) and the Radiation Oncology Mater Centre (ROMC), Queensland Health. Computational resources used in this work were provided by the HPC and Research Support Group, QUT.

References

[1] Costa M J, Delingette H, Novellas S and Ayache N 2007 *Proc. 10th Int. Conf. on Medical Image Computing and Computer Assisted Intervention (Brisbane)* part I LNCS **4791** (Berlin: Springer) 252–60
[2] Chen S and Radke R J 2009 *Proc. 12th Int. Conf. on Computer Vision (Kyoto)* (IEEE) 763–70
[3] Chen T, Kim S, Zhou J, Metaxas D, Rajagopal G and Yue N 2009 *Proc. 12th Int. Conf. on Medical Image Computing and Computer Assisted Intervention (London)* part I LNCS **5761** (Berlin: Springer) 43–50
[4] Zhou J, Kim S, Jabbour S, Goyal S, Haffty B, Chen T, Levinson L, Metaxas D and Yue N J 2010 *Med. Phys.* **37** 1298–1308
[5] Lu C, Chelikani S, Papademetris X, Knisely J P, Milosevic M F, Chen Z, Jaffray D A, Staib L H and Duncan J S 2011 *Med. Image Anal.* **15** 772–85
[6] Winkler G 2003 *Image Analysis, Random Fields and Markov Chain Monte Carlo Methods: A Mathematical Introduction* 2nd ed. (Heidelberg: Springer-Verlag)
[7] Kalender W A 2011 *Computed Tomography: Fundamentals, System Technology, Image Quality, Applications* 3rd ed. (Erlangen: Publicis)
[8] Alston C L, Mengersen K L, Robert C P, Thompson J M, Littlefield P J, Perry D and Ball A J 2007 *Comp. Stat. Data Anal.* **51** 4282–96
[9] Frank S J, Dong L, Kudchadker R J, de Crevoisier R, Lee A K, Cheung R, Choi S, O'Daniel J, Tucker S L, Wang H and Kuban D 2008 *Int. J. Radiat. Oncol. Biol. Phys.* **71** 813–20
[10] Besag J 1986 *J. R. Stat. Soc. Ser. B* **48** 259–302
[11] Feng D and Tierney L 2011 *J. Stat. Soft.* **44**(7)
[12] Dice L R 1945 *Ecology* **26** 297–302